Atmos. Chem. Phys. Discuss., 15, 27357–27404, 2015
www.atmos-chem-phys-discuss.net/15/27357/2015/
doi:10.5194/acpd-15-27357-2015

Atmospheric Chemistry and Physics Discussions

The impact of observation nudging on simulated meteorology and ozone concentrations during DISCOVER-AQ 2013 Texas campaign

X. Li[1], Y. Choi[1], B. Czader[1], H. Kim[2,3], B. Lefer[1], and S. Pan[1]

[1]Department of Earth and Atmospheric Sciences, University of Houston, Houston, TX, 77204, USA
[2]NOAA Air Resources Laboratory, College Park, MD 20740, USA
[3]University of Maryland, Cooperative Institute for Climate and Satellite, College Park, MD, USA

Received: 17 July 2015 – Accepted: 18 September 2015 – Published: 9 October 2015

Correspondence to: X. Li (xli@central.uh.edu)

Published by Copernicus Publications on behalf of the European Geosciences Union.

Abstract

Air quality modeling demands accurate meteorological simulations. Observation nudging, also known as objective analysis (OA), is generally considered a low-cost and effective technique to improve meteorological simulations. However the meteorological impact of OA on chemistry has not been well characterized. This study involved two simulations (with/without OA) to analyze the impact of OA on the simulated meteorology and ozone concentrations during the Deriving Information on Surface conditions from Column and Vertically Resolved Observations Relevant to Air Quality (DISCOVER-AQ) Texas campaign period in September 2013, using Weather Research and Forecasting (WRF) and Community Multiscale Air Quality (CMAQ) models. The results showed improved correlations between observed and simulated parameters from the OA case. The index of agreement (IOA) improved by about 9 % for surface temperature and 6–11 % for surface zonal (U-WIND) and meridional (V-WIND) winds when OA was employed. Analysis of a cold front event indicated that OA improved the timing of wind transition during front passage. Employing OA also reduced the model biases in the planetary boundary height predictions. For CMAQ simulated surface ozone during the whole simulated period, IOA improved by 6 % in the OA case. The high ozone episode on 25 September was a typical post-front ozone event in Houston. The small-scale morning wind-shifts near the Houston Ship Channel combined with higher aloft ozone from recirculation likely caused the day's ozone exceedance. While OA did not reproduce the wind shifts on that day and failed to reproduce the observed surface and aloft high ozone, analyses of surface and aircraft data found that OA results matched better with observations. In a two-hour period during the event, substantially better winds in OA noticeably improved the ozone. Further work on improving OA's capability to reproduce local meteorological events could enhance a chemistry model's ability to predict high ozone events.

ACPD
15, 27357–27404, 2015

1 Introduction

Accurate meteorological simulations are essential to photochemical modeling since meteorological variables, such as cloud fraction, winds, planetary boundary layer (PBL) heights and precipitation, significantly impact the production, transport, and deposition of various chemical species (e.g., Pour-Biazar et al., 2007; Banta et al., 2005; Cuchiara et al., 2014). Common approaches of improving meteorological simulations include the selection of high quality terrain and input data (e.g., Cheng and Byun, 2008), the optimization of physics and dynamics options (e.g., Zhong et al., 2007), and the implementation of four dimensional data assimilation (FDDA). The air quality modeling group at the University of Houston (UH) had performed several sensitivity studies on the various parameterization schemes in the recent past (e.g. Zhong et al., 2007; Ngan et al., 2012; Cuchiara et al., 2014).

There are several FDDA methods including nudging (e.g., Stauffer and Seaman, 2004) and Variational Methods (3D-VAR or 4D-VAR; e.g., Le Dimet and Talagrand, 1986; Huang et al., 2009). 4D-VAR obtains optimal states of the atmosphere using multi-time-level observations by globally adjusting a model solution to all available observations over an interval of time. Nudging is a simple yet flexible FDDA method originally developed by Stauffer and Seaman (1990, 1994), and implemented in the Fifth-Generation PSU/NCAR Mesoscale Model (MM5). Not intended for optimal adjustment, nudging is less computationally intensive and needs special care for the nudging coefficients. Nudging involves adding an artificial tendency term to one or more model prognostic equations that reflect the difference between the best estimate of the observed state and the model state at a given location and time. In short, the goal is to "nudge" model state towards observed state. There are several types of nudging such as 3D analysis nudging, surface analysis nudging, and observation nudging. In the case of analysis nudging, the model state is nudged toward gridded analysis. The difference between 3D and surface analysis nudging is that 3D analysis (at all model levels except for surface) data are used to improve 3D fields while surface analysis

ACPD
15, 27357–27404, 2015

data are used to improve surface fields. In observation nudging, the model is perturbed such that its predictions match better with observations at individual locations, both on surface and aloft. The MM5 nudging codes were later improved and incorporated into the Weather Research and Forecasting (WRF) model by Liu et al. (2005, 2006). The enhancements enable observation nudging to assimilate a large variety of direct or derived observations.

The benefit of applying nudging to improve meteorological simulations has been demonstrated in many studies (e.g., Deng, 2009; Gilliam and Pleim, 2010). However, only a few have extended the investigation into chemistry simulations. Otte (2008) showed that analysis nudging is able to improve MM5 meteorology, as well as Community Multiscale Air Quality (CMAQ) chemistry as reflected in ozone statistics. Better "model skill" scores were achieved for daily maximum 1 h ozone mixing ratio after analysis nudging over a 35-day period. Byun et al. (2008) performed over a dozen tests on observation nudging (with analysis nudging turned on) and showed observation nudging improved both winds and temperature in MM5 simulations. The study also gave an example in which improved wind fields on a given day led CMAQ to better capture the high ozone area southwest of Houston. Ngan et al. (2012) compared results from several MM5-CMAQ simulations and showed that fully nudged (with both analysis nudging and observation nudging implemented) simulations outperformed a forecast run in both meteorology and chemistry. Their study location was Houston Texas, the same as in this study. No detailed statistics were presented on the quantitative improvements from the nudging. Previous work by the current authors (e.g., Rappenglueck et al., 2011; Czader et al., 2013) showed that observation nudging helps to correct errors in model wind fields, which are critical to the transport process of air pollutants, as well as the production of secondary pollutants. To the best of the authors' knowledge, there is no comprehensive existing study on the impact of observation nudging on chemistry, especially when the meteorological model is WRF. This study intends to fill up the gap by investigating the sensitivity of WRF-CMAQ simulations to the use of observation nudging. Although not elaborated here, the WRF-CMAQ sensitivity to dif-

ACPD
15, 27357–27404, 2015

ferent observation nudging frequencies was also explored. In theory, higher frequency of observation nudging input should have a higher probability to capture small scale events, such as local wind shifts. These events may only slightly impact local weather, yet they can have a large effect on chemistry since it is well-known that local stagnation and wind convergence/reversals can contribute to the pollutant build-up (e.g., Banta et al., 1998; Cheung and Wang, 2001; Tucker et al., 2010).

There is a significant presence of petro-chemical facilities, power plants and motor vehicles in the Houston-Galveston-Brazoria (HGB) region located in southeastern Texas (SETX). The major pollutant in the region is ozone due to the abundant emissions of precursors like nitrogen oxide (NO_x) and Volatile Organic Compounds (VOCs). During the long and hot summer, ozone often rises above the threshold level as stipulated in the National Ambient Air Quality Standards (NAAQS). Consequently HGB has been designated as an ozone non-attainment region by the US Environmental Protection Agency (USEPA). The petro-chemical plants are largely concentrated in the Houston Ship Channel (HSC) area – just north of the Galveston Bay. The VOCs emitted from the HSC area are highly reactive and have been shown to contribute greatly to the high ozone episodes in HGB (e.g. Kleinman et al., 2002; Daum et al., 2003). Depending on the local meteorology, the plumes from HSC may be carried to different locations in HGB and trigger high ozone events on its path. Metropolitan Houston has a high level of NO_x emissions partly due to heavy vehicular traffic in the city. As a result of the large amount of precursor emissions and favorable weather, relatively frequent high ozone events occur in the area. Ngan and Byun (2011) gave an analysis on the relationships between the high ozone frequency and underlying weather patterns. They derived the weather patterns from a classification scheme using large-scale 850 hPa synoptic flow as input.

The Houston-Galveston-Brazoria region has been the location of interest of many air quality studies (e.g., Banta et al., 2005; Parrish et al., 2009; Lefer and Rappengluck 2010; Olaguer et al., 2013; Czader et al., 2013, Choi et al., 2012; Choi, 2014; Choi and Souri, 2015; Pan et al., 2015). It is a good place for studying ozone production

ACPD
15, 27357–27404, 2015

and transport due to the existence of a dense surface monitoring network, as well as several intensive measurement field campaigns which provide ample observational data. For example, in September 2013, the National Aeronautics and Space Administration (NASA), joined by a number of agencies and universities, conducted a field measurement campaign in SETX as part of its the Deriving Information on Surface conditions from Column and Vertically Resolved Observations Relevant to Air Quality (DISCOVER-AQ) program. The NASA program has conducted air quality and meteorology measurements at several different locations in the U.S. The availability of dense surface observations is important in OA's capability to correct erroneous local winds in the model. Without a rich set of observations, the performance of OA will be handicapped.

This study involved performing two WRF-CMAQ simulations for the 2013 DISCOVER-AQ Texas time period in order to understand the impact of observation nudging using comprehensive sets of observation data from both in-situ surface and aircraft measurements. We evaluated model performance and calculated statistics for both WRF and CMAQ. Meteorological fields critical to ozone chemistry were examined to explore the model sensitivity to OA. The paper is structured as following: Sect. 1 is introduction; Sect. 2 describes the measurement data and the modeling system; Sect. 3 covers the evaluation protocols; Sect. 4 discusses the general meteorological conditions that occurred during the campaign period; Sect. 5 presents the modeling results, and Sect. 6 provides discussions and conclusions.

2 Observational data and model configurations

For evaluation of the results, this study used regular measurements from the Continuous Ambient Monitoring Station (CAMS), operated by the Texas Commission on Environmental Quality (TCEQ), as well as PBL and aloft ozone measurements from DISCOVER-AQ campaign. For observation nudging, in addition to the CAMS data sets,

ACPD
15, 27357–27404, 2015

several datastreams from the Meteorological Assimilation Data Ingest System (MADIS) were also used.

2.1 Observational data

The CAMS measurement network collected real-time meteorology and chemistry data. The measured parameters differ from station to station. The station density at SETX is relatively high. There are 63 sites having meteorological measurements and 52 sites having ozone measurements in 4 km domain (Fig. 1) during DISCOVER-AQ time period. The stations are represented by dots, with La Porte (C556) site labeled. All CAMS observations are accessible at TCEQ website: http://www.tceq.state.tx.us/cgi-bin/compliance/monops/daily_summary.pl.

Additionally, PBL height measurements for September were obtained from a team at University of Houston, which employed LIDAR (Light Detection and Ranging) to detect the PBL height. Presently, only data at one site is available.

For analysis of ozone aloft on 25 September, we also used measurements from aircraft P-3B, part of the rich datasets collected during DISCOVER-AQ campaign (http://www-air.larc.nasa.gov/missions/discover-aq/discover-aq.html). The P-3B data had over 100 parameters and are accessible from the website.

2.2 Model configurations

The modeling system consists of WRF-SMOKE-CMAQ models as described in the following three subsections. Two sets of simulations, with the only difference in whether OA was adopted, were performed. The base case, referred as "No-OA", did not employ observation nudging. The second case, "1Hr-OA", performed observation nudging using hourly observation input.

ACPD
15, 27357–27404, 2015

2.2.1 WRF configurations

Both WRF simulations used the same nested domain and NARR (North American Regional Reanalysis) as input, with grid nudging turned on.

Domain setup

Figure 2 depicts the horizontal domain setup. There were two nested domains, with 12 and 4 km resolution. The 4 km domain covered SETX and a small portion of Louisiana. The 12 km domain (red box) encompassed Texas and a few neighboring states (or parts). The grid sizes for the 12 and 4 km domains were 161 × 145 (E–W by N–S), and 95 × 77 respectively. The projection type is Lambert conic conformal (LCC). Three projection parameters, first latitude, the second latitude and the standard longitude, are 33° N, 45° N and 97° W degrees respectively. The USEPA used the same projection parameters to develop emission inventories for air quality modeling. Vertically both domains had 27 eta layers based on dry hydrostatic pressures. The model top is set to be 100 hPa, corresponding to top layer pressure of the input NARR data.

Input data

Both WRF simulations were retrospective runs using NARR analysis as input, downloadable from: http://rda.ucar.edu/datasets/ds608.0/. The NARR data were based on an Eta 221 grid at 29 pressure levels. Its horizontal resolution was 32 km and the frequency was 3 h. The initial and boundary conditions were generated from the NARR analysis by WRF. An alternative to NARR was the Eta-NAM analysis data. However, the data temporal frequency was lowered from 3 to 6 h starting 2013. Our test showed that it was not as good as NARR for WRF input, likely because of lower temporal resolution.

ACPD
15, 27357–27404, 2015

Physics and FDDA options

Major physics options were listed in Table 1. These options are consistent with the WRF options in our daily air quality forecasting system (http://spock.geosc.uh.edu/). Among them, the PBL and cumulous cloud schemes are especially critical. Our past experiences demonstrated that Yonsei University (YSU) is the best PBL scheme in Houston case study while Kain-Fritsch (K-F) is the preferable cumulous scheme. The choice of YSU scheme is also corroborated recently by Cuchiara et al. (2014). K-F scheme is "drier" than others and produces less bogus convectional thunderstorms. The numbers in parentheses represent the value of corresponding namelist variable in WRF's namelist file. For example, the "1" after YSU is the value of the namelist variable "bl_pbl_physics" in WRF's namelist file. For both of the simulations, we performed standard grid nudging for both of the cases using NARR analysis. For grid nudging options, we generally followed the recommendations in WRF's User Guide. For example, the mass fields (temperature and moisture) were nudged only at layers above the PBL while wind fields were adjusted at all layers including the surface layer.

Observation nudging with MADIS and CAMS data in WRF

As mentioned in the introduction, observation nudging is regarded as a low-cost and effective method for improving meteorological model performance, but it requires additional observational data. In this study, we acquired the input observation data and generating files in "little_r" format using similar procedures found in Ngan et al. (2012) and Czader et al. (2013). Observational data came from the MADIS and TCEQ CAMS. MADIS (https://madis.ncep.noaa.gov/), a National Oceanic and Atmospheric Administration (NOAA) program, collects, integrates, quality-controls, and distributes observations from NOAA and other organizations. The four MADIS datasets used for observation nudging were NOAA Profiler Network (NPN), Cooperative Agency Profilers (CAP), Meteorological Terminal Aviation Routine (METAR) weather report and NOAA Radiosonde (RAOB). The METAR dataset was collected by mostly first-order, METAR

ACPD
15, 27357–27404, 2015

reporting, surface monitoring stations. NPN, RAOB and CAP were the most commonly used upper air datasets.

The "little_r" files from previous step were fed into WRF OBSGRID module to update the domain analyses ("met_em" files), and, generate additional surface analyses ("sffdda") and text nudging files ("OBS_DOMAIN"). Actual observation nudging was performed by the main WRF program by properly setting observation nudging namelist variables. The namelist for OBSGRID and relevant WRF section settings came largely from recommended values of WRF User's Guide and a previous study by Ngan et al. (2012).

Theoretically, observation nudging updating at a higher frequency should enhance the model's performance. A typical frequency of input analysis data is 3 h while the frequency for observational data is hourly. The 3 h frequency of input analyses may be the reason for the default 3 h time-interval in WRF's OBSGRID settings for generating the observation nudging files. Since there were few existing OA studies related to air quality and we are not aware of any reference to the adoption of 1 h input frequency, we assume that all the existing studies used the default 3 h interval. As the WRF model allows the interval to be set to 1 h or smaller when corresponding observational data were available, we tested both 1 and 3 h scenarios. The results indicated that 1 h OA had slightly better performance than the 3 h one. As a result, this study adopted 1 h temporal frequency for observation nudging.

It should be noted that the default time interval for modified gridded analyses, i.e., the "metoa-em" and "sgfdda" files have to match input analysis data in OBSGRID. The namelist variable was called "interval", with a default value of "10800" s. The time-interval for output nudging files was set by namelist variable "int4d", with the same default value of "10800" s. To output the observation nudging files hourly, "int4d" should be set to "3600" s. This means that the OBSGRID output files, "metoa_em" and "OBS_DOMAIN", did not have the same interval in our study.

In WRF, there were a few namelist variables controlling the frequency of grid nudging and observation nudging. The first one was "interval_seconds", which

ACPD
15, 27357–27404, 2015

should match the interval of input grid nudging files ("met-em"). The second one was "sgfdda_interval_m", matching the interval of surface grid nudging files ("sgfdda"). In our simulation, both intervals were equal to 3 h. The third one was "auxinput11_interval", controlling the updating interval for observation nudging files ("OBS_DOMAIN"). The last one, "obs-ionf", determined the nudging frequency relative to internal integration time-step. For example, if the integration time-step for the coarse domain is 30 s, setting "obs_ionf" to 1 means performing OA every 30 s, while setting "obs_ionf" to 3 means performing OA every 90 s. In our simulation, "obs_ionf" is set to 1.

One departure from the default OA setting in WRF was that the moisture OA was turned off with "obs_nudge_mois" set to 0. This was based on our past experiences since performing moisture OA sometimes trigger excessive artificial thunderstorms which disrupted model flow fields.

2.2.2 Emission processing

For anthropogenic sources we utilized the National Emission Inventory of 2008 (NEI2008) generated by the USEPA. The mobile emissions were processed with EPA's Motor Vehicle Emission Simulator (MOVES). Using the Sparse Matrix Operator Kernel Emissions (SMOKE) Modeling System v3.1 the inventory was converted to gridded emission rates as well as to emission species as listed in the Carbon Bond 05 (CB05) chemical mechanism that is used in CMAQ modeling. The biogenic emissions were estimated using the Biogenic Emissions Inventory System (BEIS) v 3.14. Although NEI2008 might have overestimated NO_x emissions in Houston (e.g., Choi, 2012; Czader et al., 2015) which could have impacted on ozone formation in the region, we used base NEI2008 without adjustment because the adjustment of the NO_x emission also has large uncertainty. Pan et al. (2015) showed that the CMAQ ozone performance using NEI2008 appears reasonable.

ACPD
15, 27357–27404, 2015

2.2.3 CMAQ configurations

The USEPA's CMAQ (Byun and Schere, 2006) version 5.0.1 was adopted for this study, following the choice of several other Houston air quality modeling studies (e.g., Foley et al., 2010; Czader et al., 2013, 2015; Choi, 2014; Pan et al., 2015). CMAQ horizontal domains were slightly smaller than the WRF counterpart in order to avoid the discontinuity near the domain boundary. The domains were shown in Figure 2 as green and brown boxes. The chemical boundary conditions for all the species in the 4 km domain were derived from 12 km domain air quality forecasting results (http://spock.geosc.uh.edu). Vertically, CMAQ inherited the same layers from WRF without layer collapsing. Major CMAQ configurations were described in Table 2. The texts in the parentheses were the values in the CMAQ build script.

Chemical processes were simulated with the available in CMAQ CB05 chemical mechanism with active chlorine chemistry, updated toluene mechanism. For aerosol modeling, the fifth-generation CMAQ aerosol mechanism (AE5) with sea salt is selected. Cloud/aqueous chemistry is included. The total number of included species is 132, with 70 reactive gas-phase, 49 aerosol and 13 non-reactive species.

3 Evaluation metrics

To assess model performance against observations, we computed a set of five statistics including Pearson correlation, index of agreement (IOA, Willmott, 1981), mean bias (MB), root mean square error (RMSE), and Mean Absolute Error (MAE), similar to Li et al. (2008). The goal is to have a comprehensive comparison between model and observation time series. These statistics have been frequently used for performance evaluation in modeling community.

The set of five statistics was divided into three groups:

1. Measuring the direct departure of model results from observation, in measurement units

ACPD
15, 27357–27404, 2015

- Mean Bias (MB)
- Mean Absolute Error (MAE)
- Root Mean Square Error (RMSE)

2. Measuring how close the model values follow changes in the observations, unitless
   - Correlation
3. A composite performance index, index of agreement (IOA or d) suggested by Willmott (1981), unitless

IOA is considered a better performance index than correlation as it takes into account the difference in the means and standard deviation. For example, when correlations are similar, lower model biases would yield higher IOA values.

Additionally, the mean and the standard deviation (SD) of model values and observations were included as a reference.

4 General meteorological and ozone conditions in September 2013

The weather during the September 2013 simulation period was relatively dry with mostly southerly, easterly or southeasterly winds. From 5 to 19 September (all dates are in MM/DD format), there was a lack of influence of strong synoptic weather systems. Shifting wind patterns were observed during the period: light northeasterly in the early morning gradually turned clockwise to southeasterly in the afternoon and evening hours. In this period, winds shifted from southeast to near east and there were more clouds after 9 October. The only cold front arrived on the early morning of 21 September. Figure 3 shows the daily regional average temperatures and periods marked with temperature drop. Although not very significant to photochemistry, temperature drop is usually a good proxy for the critical factors affecting ozone production or transport such as cloudiness, wind, and precipitation.

ACPD
15, 27357–27404, 2015

Rain events occurred on 2, 10, 16, 19 to 21 and 28 to 30 September. None of them was heavy. The 20 and 21 September events consisted of widespread light to medium showers. Besides the above-mentioned dates, there were a few other days with sporadic drizzles.

A majority of the days between 1 and 20 September were mostly sunny to mostly cloudy. The periods from 8 to 10 September and 18 to 20 September had more clouds than other days. The period from 21 to 30 Spetember was influenced by a cold front passage. The days between 22 and 24 September were sunny and cool. Then the surface wind reversed direction during mid 25 September and brought clouds back from 26 to 30 September.

In SETX, high ozone events in fall season were typically associated with a passage of cold front (e.g., Rappenglueck et al., 2008). The only ozone event with hourly surface ozone exceeding 120 ppb (parts per billion) in September, which occurred on 25, fell in this category.

Figure 4 shows the daily regional averaged ozone. On most days, the observed averaged ozone fell below 30 ppb. Since the winds after dawn consistently pushed the precursors from the industrial area to the southwest of the city, the wind pattern did not favor the local ozone production. The daytime winds also contained a persistent easterly component which moved the pollutants away from the Houston metropolitan area. In the first 10-day period, less background ozone originated from the Gulf of Mexico contributed to the low-ozone days. With overcast skies on 19 and 20, ozone values dipped below 20 ppb. The two highest ozone days, characterized by post-frontal ozone events, were the 25th and the 26th.

5 Evaluation of simulation results

To evaluate the WRF simulation, we calculated statistics for surface temperature and winds in the 4 km domain. For PBL heights, we chose to plot out the time-series for the one site we had observations due to significant amount of missing data (data coverage

ACPD
15, 27357–27404, 2015

is about 50 %). For CMAQ evaluation, we calculated the surface ozone statistics for the whole month. Also, we plotted vertical ozone profile and calculated biases for ozone aloft on 25 September.

5.1 Meteorology

5.1.1 Temperature

The comparison of regional averaged daily temperatures for the analyzed time period is shown in Fig. 3. The regional averaged daily temperature was calculated by averaging the hourly temperature from ~60 CAMS sites in the 4 km model domain. Despite the differences in the days with more clouds/precipitation, the simulated averaged temperatures tracked the in-situ data very well. It was also evident that the "1Hr-OA" case matched better with the observations, especially for 20–23 September.

The statistics of hourly surface temperature are presented in Table 3. With higher IOA and lower mean biases (MB), the "1Hr-OA" case was clearly better than the base case "No-OA". The IOA of "1Hr-OA" was about 9 % higher than the base case.

5.1.2 Winds

Wind fields are known to significantly affect chemistry (e.g., Banta et al., 2005, 2011; Darby, 2005). In ozone chemistry, winds affect the accumulation of precursors and hence the resulting ozone production. Winds are also responsible for dispersing high ozone and bringing background ozone. In HGB, prevailing southerly to southeasterly winds in the summer time significantly lowered the ozone level in the metro area. Therefore, high ozone events usually occur when such wind pattern changes. Cold front intrusion, coming as early as late August, blows pollutants to the south. As a result, an area of high ozone develops in the Gulf. A few days later, cold fronts weaken and reversing winds bring ozone back. High ozone also occurs during intra-day pollutant recirculation events when pollutants previously blown away from industrial zone are brought back

ACPD
15, 27357–27404, 2015

by reversing winds. The high ozone event in the HSC area on 25 September was likely due to a combination of local recirculation caused by onset of the bay breeze and increased background ozone brought in by the much-larger scale southerly flow from the Gulf.

Due to the land-water thermal contrast and the different size of the Galveston Bay and the Gulf of Mexico, the western shore of the Galveston Bay often experiences a successive onset of bay breeze and sea breeze in the summer. The bay breeze is typically a weaker easterly while sea breeze is a stronger southeasterly. Sea breeze usually comes one to a few hours later after the bay breeze. The bay breeze and the subsequent sea breeze phenomena in Houston were described by Banta et al. (2005).

The statistics of zonal (*U*-WIND) and meridional (*V*-WIND) wind components are listed in Table 3. The purpose of choosing *U* and *V* over wind speed and direction is to avoid the anomalies in the wind direction statistics. For example, although wind direction of 5 and 355° are close, the statistics suggest that they are distinctively different.

For both *U* and *V* components of wind, "1Hr-OA" had higher correlation and IOA than "No-OA". The model performance on *U* and *V* are similar, with the correlation in a range of 0.76 to 0.81 for all the cases. As a reference, the performance of the OA case ("M1") in Ngan et al. (2012) is very close to that in this study, with a correlation of 0.75 for *U* and 0.82 for *V*. In terms of IOA, the OA case had a larger lead over the base case, ahead by 5–6 % in *U* and 10–11 % in *V* over the base case. This can be explained by the much reduced wind biases in the OA case.

The base case had consistently stronger winds, especially the southerly component, than the observation. This was reflected in the mean bias "MB", as well as the model mean "M_M". Winds were reduced significantly after OA was performed. Interestingly, the high southerly bias in "No-OA" turned slightly negative after OA. Winds originating from the Gulf were also stronger in base case, which played a role in raising the ozone level in the area. Figure 5 illustrated the slowing down of southerly winds after observation nudging. As a result, winds matched better to the observations.

ACPD
15, 27357–27404, 2015

5.1.3 PBL height

Atmospheric pollutants are largely confined in the PBL as most of the emissions sources are close to the ground level. PBL plays a critical role in mixing and spreading the pollutants. Haman et al. (2014) studied the relationship between ozone level and PBL height at a Houston CAMS site and found that nighttime and early morning PBL heights were consistently lower on high ozone days than on low ozone days. Czader et al. (2013) pointed out that the model underprediction of PBL during nighttime may have caused the CO overprediction at the same site. CO is a good proxy for understanding model's transport since it has low reactivity and a relatively long life time in the troposphere.

Cuchiara et al. (2014) conducted four WRF/Chem sensitivity tests on the PBL schemes over southeast Texas. While no preferred PBL scheme was identified for WRF simulations, the Yonsei University (YSU) scheme outperformed others in ozone prediction. As a note, we used YSU in this study as it had been tested in the past and the study by Cuchiara et al. (2014).

The PBL height data were taken at an urban site very close to CAMS site C695, located on University of Houston campus. A study by Haman et al. (2012) showed that Houston's daily maximum PBL height reached its highest values of slightly over 2000 m in August. In September, typical daily maximum PBL height was 1500 m at 15 CST while daily minimum was just below 200 m between 00 CST and 06 CST. The comparison of observed and model PBL height is shown at Fig. 6. The model tended to overpredict the daily maximum and OA helped to reduce the overpredictions. For the daily minimum PBL height, "No-OA" had slightly high biases while the OA case matched quite well with observations. The observed minimum PBL height was lower than that reported by Haman et al. (2012), likely due to the cloudy condition in September 2013. There was no apparent explanation on the reduced daytime PBL biases in the OA case than the base case, but it is likely the results of improved winds and temperatures in PBL.

ACPD
15, 27357–27404, 2015

Cold front passage

The surface winds on 20 Spetember were overwhelmingly southerly in the region and reversed on 21 Spetember due to the arrival of a cold front. The hour-by-hour wind shifts for 11 sites in HGB on 21 Spetember are plotted in Fig. 7. The sites are sorted by latitude with the southernmost site, Galveston C1034, located at the bottom row. There was only one site, Deer Park C35, showing weak southerly at 00 CST while all the others had mostly weak northerly. Starting from 01 CST, winds in the entire HGB area turned northerly to northeasterly and continued gaining strength in the next few hours, indicating cold air had taken over the region.

Both cases performed reasonably well on 21 Spetember and the timing of wind shift was captured quite accurately although "No-OA" lagged about an hour. The winds turned weak northerly at 00 CST for most sites and "No-OA" still showed all southerly. Besides the timing, OA also helped moderate the winds as the northeasterly winds in "No-OA" case sometimes were too strong. The V-wind bias on 21 September is reduced from -2.5 to $-0.6\,\mathrm{m\,s^{-1}}$ after OA was performed. The performance of the OA case during cold front passage was consistent with our past simulations.

5.2 Ozone

5.2.1 Regional daily average ozone

Figure 4 showed the regional average daily ozone, which was defined similarly to averaged daily temperature. Regional averaged daily ozone provides a global view on model's performance. Model failure of daily averaged ozone (such as wrong trend or too high bias) was often a sign of model flaws. For example, a consistently high ozone bias could mean either the model background ozone or the emission of the precursors are too high. On the other hand, if the high biases are present only at certain days, then it is likely a meteorological problem than issues in model background or emission

ACPD
15, 27357–27404, 2015

inventory. Overall ozone level was low and model did well on the daily trend although positive biases were seen for some days.

Although model had high biases for majority of the days, biases were consistently lower for the OA case during two periods: 7 to 9 Spetember and 17 to 21 Spetember. The reduced biases were likely due to the lower southerly winds in the OA case since model had higher background ozone originated from the Gulf.

In Fig. 4, the first three orange circles showed the days with high model biases. The first two circles consisted of days with lower than "normal" background ozone. Since model ozone had fixed boundary values, model was unable to capture the daily ozone variation at the boundary. The third circle consisted of days with overcast skies. The high model biases were likely the result of problems in model's cloud fields and high background ozone values. A future study to upgrade the accuracy of cloud fraction using remote sensing data (e.g., MODIS) should be helpful in explaining the biases.

There were a few days with elevated ozone due to post-front meteorology conditions. The only exceedance happened on 25 Spetember, which was likely caused by meteorological events in Houston and the Galveston Bay. Averaged ozone on 09/26 was slightly higher after southerly winds transported back the ozone from the Gulf, raising the ozone level in the entire region. A more detailed analysis of model predictions on 25 and 26 Spetember will be presented in the following section.

5.2.2 Performance statistics

The ozone statistics were displayed in Table 4. Both cases had very close correlation of 0.72 and 0.73. However, the mean biases in the OA case were lower by 3.2 ppb, which helped raise the IOA from 0.78 to 0.83. The model standard deviation increased in the OA case and matched better with observation. The improvement in IOA was slightly less in temperature and winds.

ACPD
15, 27357–27404, 2015

5.2.3 High ozone episode after the passage of a front

In SETX, high ozone events during the fall season usually occurred after the passage of a cold front (e.g., Rappenglück et al., 2008; Ngan and Byun, 2011; Ngan et al., 2012; Haman et al., 2014). Two factors may have contributed to the post-front ozone events: (1) following a cold spell winds reverse direction and subsequent light winds and sunny skies create an ideal condition for ozone production and accumulation (2) wind reversal transports back the pollutants that were blown into the Gulf previously, a phenomenon commonly known as recirculation.

During the DISCOVER-AQ period, the two days with highest ozone were 25 September and the day 26 September (Fig. 4), but the two days exhibited different patterns. The 1 h maximum ozone on 25 September was localized and higher by about 40 ppb. In addition to heightened background ozone, the major contributor was the production resulting from favorable weather conditions: sunny, overall light winds and shifting winds over the industrial area. The light morning land breeze carried pollutants from ship channel area to the Galveston Bay. As the day warmed up, bay breeze started to develop and carry pollutants back to the land. This localized circulation was described by Banta et al. (2005). Ngan et al. (2012) reported the same phenomenon in their Texas Air Quality Study-II 2006 study. 26 September is characterized by elevated background ozone from early morning to late night.

Figure 8 shows the ozone time series of La Porte (C556), located in HSC area (Fig. 1). In September, the highest hourly ozone of 151 ppb occurred at C556 at 13 CST of 25 September. From 9 CST to 12 CST, ozone rose from 10 to 150 ppb. The large increase in ozone was the result of chemical production under favorable meteorological condition in an area with accumulated precursors. Figures 9 and 10 depict the wind and ozone concentrations at 08 CST and 13 CST.

From the wind plots of Fig. 9, we can see that the winds at 8 CST were light northerly for sites located on the north side while winds were mostly westerly for the sites in the middle and south. The base case winds were all northerly while OA case had northwest

ACPD
15, 27357–27404, 2015

winds for north side and west winds for the middle and south. The winds in OA case were much more realistic. The 9 CST winds were similar to those of 8 CST. As a result, the ozone statistics in Table 5 showed that the OA case had much better correlation and IOA than the base case during 8–9 CST. This example demonstrated OA's ability to correct erroneous winds. However, later events showed OA may not always be able to perform consistently.

The bay breeze started to develop at 10 CST near C556. The early onset was likely to be related to the warming up the previous afternoon on 24 September (Fig. 3). At 10 CST most other sites to the west of HSC experienced light northwest winds while winds at HSC were from northeast. Combined with the easterly bay breeze, a convergence zone was formed just below C556, where emissions from the HSC area stalled and accumulated. At 13 CST, the whole region had light winds and the bay breeze was well developed. The highest ozone indeed appeared in C556 and its vicinity. The rapid increase of ozone concentration for C556 between 9-13 CST is shown in Fig. 8.

It is important to note that both modeled cases missed the wind shifts in the HSC area, and the resulted convergence zone near C556. This could explain the model's inability to recreate the sharp ozone increase at C556. Figure 9 shows that the ozone level around HSC area is quite low ($\sim$ 10 ppb) at 08 CST. A further examination showed that while both model cases missed the wind shift and convergence, though the patterns were different. The base case had flawed winds for most of the morning: instead of a weak northwesterly, it had stronger northeasterly. By 08 CST, winds were almost uniformly northerly in the base case while they were weak west-northwesterly in the OA case (Fig. 9). The oval in Fig. 9 top-left panel shows the mismatch of winds around C556 in the base case. As a result, the NO_x produced in the city was carried further to the southeast in the model in the base case. Until 13 CST, base case winds did not shift directions by much. The OA case got the early hour weak northwesterly right, but missed the bay breeze onset between 10 and 13 CST (oval in Fig. 10). The OA case could not reproduce the small-scale wind reversal near C556, suggesting there is a

ACPD
15, 27357–27404, 2015

limitation in current WRF OA's capability. On the other hand, the OA case did improve the spatial ozone pattern, as the high ozone area was closer to HSC after OA (Fig. 10).

The ozone measurements from aircraft P3-B provided a more complete picture for 09/25's ozone evolution. During the day, P-3B flew around the industrial area, Galveston Bay, and Galveston Island for about 9 h. Figures 11 and 12 showed ozone concentrations along aircraft tracks at 08 and 13 CST, with surface layer ozone from the "No-OA" case as background. The background was only intended as a reference. At 08 CST, ozone level of 60–80 ppb aloft was already observed at three locations (three loops in Fig. 11): Galveston Island, Smith Point and inner city. Another high of ~ 90 ppb could be seen above the HSC area. Ozonesonde observations over HGB showed the ozone aloft were normally ~ 40–50 ppb (e. g., Li and Rappengluck, 2014). The higher-than normal ozone aloft suggested a post-front ozone recirculation condition. Such high ozone aloft might raise surface ozone level as a growing PBL downwardly mixed the air aloft with near surface air. At 13 CST, high ozone over 100 ppb was observed at multiple locations. The highest ozone aloft, ~ 160 ppb, occurred southwest of Smith Point in the Galveston Bay. Such level of ozone increase was likely the result of active production in the industrial zone and around Galveston Bay.

Figure 13 shows hourly ozone vertical profiles from 08 CST to 16 CST of 25 September, with ozone being displayed on the x-axis and height on the *y* axis. One observation dot was averaged over all the grid cells in the same model layer. For example, during 08-09 CST, aircraft flew passing 30 cells at model's 5th layer. The 5th layer had a mid-layer height of 287.5 m. The averaged ozone of the 30 cells was 56 ppb. It should be noted that the observed ozone was averaged over multiple measurements in the same model cell, such that they could be properly compared to model values. The 08 and 09 CST profiles showed there was a high ozone layer with average ozone of ~ 65 ppb, stretching from 450 to 1200 m height. In comparison, all model runs had lower ozone in this layer. The model biases, as shown in Fig. 14, were about −10 ppb at 08 CST and grew to −20 ppb at 09 CST. The observed ozone rose continuously in following hours yet model simulated ozone stagnated around 60 ppb from surface up to 2000 m until 15

ACPD
15, 27357–27404, 2015

CST. At 16 CST, the ozone of OA case in 0–1 km layer rose 20 ppb over previous hours yet the base case ozone increased only a few ppb. Although different in magnitude, ozone aloft had a few similar features to the surface ozone. Firstly, the model missed the observed high ozone in the afternoon by a large margin. For example, the base case underpredicted 0–1 km level ozone by up to 50 ppb. The primary cause for the lower ozone production was likely model's wind fields as both model and observation had clear sky in industrial area and Galveston Bay. Secondly, nudging clearly helped reducing the ozone biases aloft. In most plots of Figure 14, the OA case had lower biases than the base case. The largest difference was at 16 CST, when nudging reduced biases from ∼ 45 to ∼ 30 ppb in the 300–1000 m layer.

6 Conclusions and discussions

In this study, we performed two Weather Research and Forecasting (WRF) and Community Multiscale Air Quality (CMAQ) model simulations to explore model sensitivity to observation nudging. In evaluating meteorological and ozone conditions, we found that objective analysis (OA) improved the meteorology and ozone performance as shown in the index of agreement (IOA) of temperature, winds, and ozone. While the base case winds were overall well simulated, observation nudging significantly reduced the high wind biases (especially the meridional wind) shown in the base case. For planetary boundary layer height, OA reduced high biases in both daily maximum and daily minimum values. In the end, the combined changes in meteorology lowered the ozone biases by about 3 ppb, a 35 % reduction. There were short time periods (such as between 07 and 09 CST on 09/25) the base case model winds differ greatly from observation and OA significantly corrected the problems, leading to much better ozone simulation. It should be noted that the model ozone biases are also impacted by the emissions and model lateral boundary conditions.

While it is easy to understand the improvements in temperature and winds after OA was applied, it is more difficult to explain how other variables such as PBL and clouds

ACPD
15, 27357–27404, 2015

reacted to OA. The indirect impact of these meteorological variables on ozone was harder to assess. In our study, we did not evaluate clouds quantitatively as there were no digitized cloud fraction data available for our modeling domains. A preliminary analysis on convection showed that there were occasions in which model missed the convection or precipitation and there were other occasions in which model created artificial convection. The convection cells were usually visible as "star-burst" from surface wind vector plots – arrows going out to different directions from a center. However, the mismatch in convection appeared to be not a serious issue since only a few occurrences were observed in the month of September.

The only high ozone episode in the simulation period was related to the cold front passage. The small-scale winds and high ozone aloft on 25 September, likely contributed to the ozone exceedance in the area. Since the maximum surface ozone at La Porte was much higher than the morning-time ozone aloft, the active local ozone production was likely the dominant factor. Analyses of ozone aloft on 25 September showed while there was high ozone aloft and large negative model biases, the OA case tended to have smaller biases, especially in late hours.

Small-scale meteorological events are frequently cited for their contributions to high ozone events. Model's capability in reproducing these events is critical in simulating such high ozone episodes. The base case did not recreate the 25 September small-scale events likely due to the complex winds and a lack of local information which can be used to steer model state closer to reality. On the other hand, the inability of the OA case to replicate the local winds is likely a result of the imperfection of the nudging process which requires further investigation. An ongoing study by the current authors suggests that errors in the metrological fields from the default grid nudging files are important sources. Methods are being tested to improve the quality of grid nudging files. In addition, more observational data (e.g., more sites and higher data frequency) and more testing on the combination of OA setting should help improve the OA performance.

ACPD
15, 27357–27404, 2015

Acknowledgements. The authors thank Texas Air Research Center (TARC) for its support through grant number 413UHH0144A and Air Quality Research Program (AQRP) through 14-014, the DISCOVER-AQ team for the aircraft data, Vanessa Caicedo for LIDAR data, and the TCEQ CAMS site team for the in-situ ozone and meteorological data.

References

Banta, R. M., Senff, C. J., White, A. B., Trainer, M., McNider, R. T., Valente, R. J., Mayor, S. D., Alvarez, R. J., Hardesty, R. M., and Parrish, D.: Daytime buildup and nighttime transport of urban ozone in the boundary layer during a stagnation episode, J. Geophys. Res.-Atmos., 103, 22519–22544, 1998.

Banta, R. M., Senff, C. J., Nielsen-Gammon, J., Darby, L. S., Ryerson, T. B., Alvarez, R. J., Sandberg, S. R., Williams, E. J., and Trainer, M.: A bad air day in Houston, B. Am. Meteorol. Soc., 86, 657–669, doi:10.1175/bams-86-5-657, 2005.

Banta, R. M., Senff, C. J., Alvarez, R. J., Langford, A. O., Parrish, D. D., Trainer, M. K., Darby, L. S., Hardesty, R. M., Lambeth, B., Neuman, J. A., Angevine, W. M., Nielsen-Gammon, J., Sandberg, S. P., and White, A. B.: Dependence of daily peak O_3 concentrations near Houston, Texas on environmental factors: Wind speed, temperature, and boundary-layer depth, Atmos. Environ., 45, 162–173, doi:10.1016/j.atmosenv.2010.09.030, 2011.

Byun, D. and Schere, K. L.: Review of the governing equations, computational algorithms, and other components of the models-3 Community Multiscale Air Quality (CMAQ) modeling system, Appl. Mech. Rev., 59, 51–77, doi:10.1115/1.2128636, 2006.

Byun, D., Ngan, F., Li, X., Lee, D., and Kim, S.: Analysis of Air Pollution Events in Summer 2006 and Preparation of Model Input Data for the Assessment Study, Grant No. 582-5-64594-FY07-02, Final Report: Evaluation of Retrospective MM5 and CMAQ Simulations of TexAQS-II Period with CAMS Measurements, Texas Commission on Environmental Quality, February, 25 pp., 2008.

Cheng, F. Y. and Byun, D. : Application of high resolution land use and land cover data for atmospheric modeling in the Houston-Galveston metropolitan area, Part I: Meteorological simulation results, Atmos. Env., 42, 7795–7811, doi:10.1016/j.atmosenv.2008.04.055, 2008.

Cheung, V. T. and Wang, T.: Observational study of ozone pollution at a rural site in the Yangtze Delta of China, Atmos. Env., 35, 4947–4958, 2001.

ACPD

15, 27357–27404, 2015

Choi, Y.: The impact of satellite-adjusted NO_x emissions on simulated NO_x and O_3 discrepancies in the urban and outflow areas of the Pacific and Lower Middle US, Atmos. Chem. Phys., 14, 675–690, doi:10.5194/acp-14-675-2014, 2014.

Choi, Y. and Souri, A.: Chemical condition and surface ozone in large cities of Texas during the last decade: observational evidence from OMI, CAMS, and Model Analysis, Remote Sens. Environ., 168, 90–101, doi:10.1016/j.rse.2015.06.026, 2015.

Choi, Y., Kim, H., Tong, D., and Lee, P.: Summertime weekly cycles of observed and modeled NO_x and O_3 concentrations as a function of satellite-derived ozone production sensitivity and land use types over the Continental United States, Atmos. Chem. Phys., 12, 6291–6307, doi:10.5194/acp-12-6291-2012, 2012.

Cuchiara, G. C., Li, X., Carvalho, J., and Rappenglück, B.: Intercomparison of planetary boundary layer parameterization and its impacts on surface ozone concentration in the WRF/chem model for a case study in Houston, Texas, Atmos. Environ., 175–185, doi:10.1016/j.atmosenv.2014.07.013, 2014.

Czader, B. H., Li, X. S., and Rappenglueck, B.: CMAQ modeling and analysis of radicals, radical precursors, and chemical transformations, J. Geophys. Res.-Atmos., 118, 11376–11387, doi:10.1002/Jgrd.50807, 2013.

Czader, B. H., Choi, Y., Li, X., Alvarez, S., and Lefer, B.: Impact of updated traffic emissions on HONO mixing ratios simulated for urban site in Houston, Texas, Atmos. Chem. Phys., 15, 1253–1263, doi:10.5194/acp-15-1253-2015, 2015.

Darby, L. S.: Cluster analysis of surface winds in Houston, Texas, and the impact of wind patterns on ozone, J. Appl. Meteorol., 44, 1788–1806, doi:10.1175/jam2320.1, 2005.

Daum, P. H., Kleinman, L. I., Springston, S. R., Nunnermacker, L. J., Lee, Y. N., Weinstein-Lloyd, J., Zheng, J., and Berkowitz, C. M.: Origin and properties of plumes of high ozone observed during the Texas 2000 Air Quality Study (TexAQS 2000), J. Geophys. Res.-Atmos., 109, D17306, doi:10.1029/2003jd004311, 2004.

Deng, A., Stauffer, D., Gaudet, B., Dudhia, J., Hacker, J., Bruyere, C., Wu, W., Vandenberghe, F., Liu, Y., and Bourgeois, A.: Update on WRF-ARW End-to-end Multi-scale FDDA System, 10th WRF Users' Workshop, Boulder, CO, NCAR, 2009

Foley, K. M., Roselle, S. J., Appel, K. W., Bhave, P. V., Pleim, J. E., Otte, T. L., Mathur, R., Sarwar, G., Young, J. O., Gilliam, R. C., Nolte, C. G., Kelly, J. T., Gilliland, A. B., and Bash, J. O.: Incremental testing of the Community Multiscale Air Quality (CMAQ) modeling system version 4.7, Geosci. Model Dev., 3, 205–226, doi:10.5194/gmd-3-205-2010, 2010.

ACPD
15, 27357–27404, 2015

Gilliam, R. C. and Pleim, J. E.: Performance Assessment of New Land Surface and Planetary Boundary Layer Physics in the WRF-ARW, J. Appl. Meteorol. Climatol., 49, 760–774, doi:10.1175/2009jamc2126.1, 2010.

Haman, C. L., Lefer, B., and Morris, G. A.: Seasonal Variability in the Diurnal Evolution of the Boundary Layer in a Near-Coastal Urban Environment, J. Atmos. Ocean. Tech., 29, 697–710, 2012.

Haman, C. L., Couzo, E., Flynn, J.H., Vizuete, W., Heffron, B., and Lefer, B. L.: Relationship between boundary layer heights and growth rates with ground-level ozone in Houston, Texas, J. Geophys. Res.-Atmos., 119, 6230–6245, 2014.

Huang, X.-Y., Xiao, Q., Barker, D. M., Zhang, X., Michalakes, J., Huang, W., Henderson, T., Bray, J., Chen, Y., and Ma, Z.: Four-dimensional variational data assimilation for WRF: Formulation and preliminary results, Monthly Weather Rev., 137, 299–314, 2009.

Kleinman, L. I., Daum, P. H., Lee, Y. N., Nunnermacker, L. J., Springston, S. R., Weinstein-Lloyd, J., and Rudolph, J.: Ozone production efficiency in an urban area, J. Geophys. Res.-Atmos., 107, 4733, doi:10.1029/2002jd002529, 2002.

Le Dimet, F. X., and Talagrand, O.: Variational algorithms for analysis and assimilation of meteorological observations: theoretical aspects, Tellus, 38A, 97–110, 1986.

Lefer, B., Rappengluck, B., Flynn, J., and Haman, C.: Photochemical and meteorological relationships during the Texas-II Radical and Aerosol Measurement Project (TRAMP), Atmos. Environ., 44, 4005–4013, doi:10.1016/j.atmosenv.2010.03.011, 2010.

Li, X. and Rappenglück, B.: A WRF–CMAQ study on spring time vertical ozone structure in Southeast Texas, Atmos. Environ., 97, 363–385, doi:10.1016/j.atmosenv.2014.08.036, 2014.

Li, X., Lee, D., Kim, S.-T., Kim, H., Ngan, F., Cheng, F., and Byun, D.: Performance Evaluation of a Year-long Run of an Air Quality Forecasting System for Southeast Texas, 10th Conference on Atmospheric Chemistry, New Orleans, January 2008, 2008.

Liu, Y., Bourgeois, A., Warner, T., Swerdlin, S., and Hacker, J.: An implementation of observation nudging-based FDDA into WRF for supporting ATEC test operations, 2005 WRF user workshop, Boulder, CO, 2005.

Liu, Y., Bourgeois, A., Warner, T., Swerdlin, S., and Yu, W.: An update on "observation nudging"-based FDDA for WRF-ARW: Verification using OSSE and performance of real-time forecasts, 2006 WRF user workshop, Boulder, CO, 2006.

ACPD
15, 27357–27404, 2015

Ngan, F. and Byun, D.: Classification of Weather Patterns and Associated Trajectories of High-Ozone Episodes in the Houston-Galveston-Brazoria Area during the 2005/06 TexAQS-II, J. Appl. Meteorol. Climatol., 50, 485–499, doi:10.1175/2010jamc2483.1, 2011.

Ngan, F., Byun, D., Kim, H., Lee, D., Rappengluck, B., and Pour-Biazar, A.: Performance assessment of retrospective meteorological inputs for use in air quality modeling during TexAQS 2006, Atmos. Environ., 54, 86–96, doi:10.1016/j.atmosenv.2012.01.035, 2012.

Olaguer, E. P., Rappengluck, B., Lefer, B., Stutz, J., Dibb, J., Griffin, R., Brune, W. H., Shauck, M., Buhr, M., Jeffries, H., Vizuete, W., and Pinto, J. P.: Deciphering the Role of Radical Precursors during the Second Texas Air Quality Study, J. Air Waste Manag. Assoc., 59, 1258–1277, doi:10.3155/1047-3289.59.11.1258, 2009.

Otte, T. L.: The impact of nudging in the meteorological model for retrospective air quality simulations. Part I: Evaluation against national observation networks, J. Appl. Meteorol. Climatol., 47, 1853–1867, doi:10.1175/2007jamc1790.1, 2008.

Pan, S., Choi, Y., Roy, A., Li, X., Jeon, W., and Souri, A.: Modeling the uncertainty of several VOC and ints impact on simulated VOC and ozone in Houston, Texas, Atmos. Environ., 120, 404–416, 2015.

Parrish, D. D., Allen, D. T., Bates, T. S., Estes, M., Fehsenfeld, F. C., Feingold, G., Ferrare, R., Hardesty, R. M., Meagher, J. F., Nielsen-Gammon, J. W., Pierce, R. B., Ryerson, T. B., Seinfeld, J. H., and Williams, E. J.: Overview of the Second Texas Air Quality Study (TexAQS II) and the Gulf of Mexico Atmospheric Composition and Climate Study (GoMACCS), J. Geophys. Res.-Atmos., 114, D00f13, doi:10.1029/2009jd011842, 2009.

Pour-Biazar, A., McNider, R. T., Roselle, S. J., Suggs, R., Jedlovec, G., Byun, D. W., Kim, S., Lin, C. J., Ho, T. C., Haines, S., Dornblaser, B., and Cameron, R.: Correcting photolysis rates on the basis of satellite observed clouds, J. Geophys. Res.-Atmos., 112, D10302, doi:10.1029/2006jd007422, 2007.

Rappengluck, B., Perna, R., Zhong, S. Y., and Morris, G. A.: An analysis of the vertical structure of the atmosphere and the upper-level meteorology and their impact on surface ozone levels in Houston, Texas, J. Geophys. Res.-Atmos., 113, D17315, doi:10.1029/2007jd009745, 2008.

Rappenglück, B., Lefer, B., Mellqvist, J., Czader, B., Golovko, J., Li, X., Alvarez, S., Haman, C., and Johansson, J.: University of Houston Study of Houston Atmospheric Radical Precursors (SHARP), Report to the Texas Commission on Environmental Quality, August 2011, 145 pp., 2011.

ACPD
15, 27357–27404, 2015

Skamarock, W. C., Klemp, J. B., Dudhia, J., Gill, D. O., Barker, M., Duda, K. G., Huang, Y., Wang, W., and Powers, J. G.: A description of the Advanced Research WRF Version 3, 1–113, 2008.

Stauffer, D. R. and Seaman, N. L.: Use of 4-dimensional data assimilation in a limited-area mesoscale model .1. Experiments with synoptic-scale data, Mon. Weather Rev., 118, 1250–1277, 1990.

Stauffer, D. R. and Seaman, N. L.: Multiscale 4-dimensional data assimilation, J. Appl. Meteorol., 33, 416–434, 1994.

Tucker, S. C., R. M. Banta, A. O. Langford, C. J. Senff, W. A. Brewer, EJ. Williams, B. M. Lerner, H. D. Osthoff, and R. M. Hardesty. : Relationships of coastal nocturnal boundary layer winds and turbulence to Houston ozone concentrations during TexAQS 2006, J. Geophys. Res.-Atmos., 115, D10304, 2010.

Zhong, S. Y., In, H. J., and Clements, C.: Impact of turbulence, land surface, and radiation parameterizations on simulated boundary layer properties in a coastal environment, J. Geophys. Res.-Atmos., 112, D13110, doi:10.1029/2006jd008274, 2007.

ACPD
15, 27357–27404, 2015

Table 1. Major WRF physics and FDDA Options, the numbers in the parentheses are the related settings in WRF namelist file.

WRF Version	V3.5.1
Microphysics	Lin et al. Scheme (2)
Long-wave Radiation	RRTMG (4)
Short-wave Radiation	New Goddard scheme (5)
Surface Layer Option	Monin-Obukhov with CB viscous sublayer scheme (1)
Land-Surface Option	Unified Noah LSM (2)
Urban Physics	None
Boundary Layer Scheme	YSU (1)
Cumulus Cloud Option	Kain-Fritsch (1)
FDDA	Grid nudging on for all; Observation-nudging on for the OA case

ACPD
15, 27357–27404, 2015

Table 2. Major CMAQ Options, the text in the parentheses are the related settings in CMAQ build script.

CMAQ version	V5.0.1
Chemical Mechanism	cb05tucl_ae5_aq: CB05 gas-phase mechanism with active chlorine chemistry, updated toluene mechanism, fifth-generation CMAQ aerosol mechanism with sea salt, aqueous/cloud chemistry
Lightning NO_x emission	Included by using inline code
Horizontal advection	YAMO (Yamartino; hyamo)
Vertical advection	WRF omega formula (vwrf)
Horizontal mixing/diffusion	Multiscale (multiscale)
Vertical mixing/diffusion	Asymmetric Convective Model (ACM) version 2 (acm2)
Chemistry solver	EBI (Euler Backward Iterative; ebi_cb05tucl)
Aerosol	AERO5 for sea salt and thermodynamics (aero5)
Cloud Option	ACM cloud processor for AERO5 (cloud_acm_ae5)
Boundary conditions	Default static profiles

ACPD
15, 27357–27404, 2015

Table 3. Statistics of surface T, U-wind and V-wind for three WRF simulations: N – data points; Corr – Correlation; IOA – Index of Agreement; RMSE – Root Mean Square Error; MAE – Mean Absolute Error; MB – Mean Bias; O – Observation; M – Model; O_M – Observed Mean; M_M – Model Mean; SD – Standard Deviation; Units for RMSE/MAE/MB/O_M/M_M/O_SD/M_SD: °C.

Surface temperature T										
Case	N	Corr	IOA	RMSE	MAE	MB	O_M	M_M	M_SD	M_SD
No-OA	41058	0.83	0.89	2.0	1.5	0.9	27.4	28.3	3.1	2.8
1Hr-OA	41058	0.94	0.97	1.0	0.8	0.0	27.4	27.4	3.1	3.1
Surface U wind										
Case	N	Corr	IOA	RMSE	MAE	MB	O_M	M_M	O_SD	M_SD
No-OA	43246	0.76	0.84	1.4	1.1	-0.6	-1.3	-1.9	1.6	1.9
1Hr-OA	43246	0.81	0.89	1.0	0.8	−0.3	−1.3	−1.6	1.6	1.6
Surface V wind										
Case	N	Corr	IOA	RMSE	MAE	MB	O_M	M_M	O_SD	M_SD
No-OA	43246	0.76	0.8	2.1	1.7	1.2	0.4	1.7	2.0	2.6
1Hr-OA	43246	0.80	0.89	1.2	0.9	-0.1	0.4	0.4	2.0	2.0

ACPD
15, 27357–27404, 2015

Table 4. Statistics of ozone for CMAQ simulations, see Table 3 for column header information.

Case	N	Corr	IOA	RMSE	MAE	MB	O_M	M_M	O_SD	M_SD
No-OA	33308	0.72	0.78	14.9	12.3	9.3	24.4	33.7	16.5	14.1
1Hr-OA	33308	0.73	0.83	13.8	11.0	6.1	24.4	30.6	16.5	17.4

ACPD
15, 27357–27404, 2015

Table 5. Statistics of ozone on 25 September 2013, all day and hour 0 to 13. Both correlation and index of agreement are unitless. The bold numbers indicate the three hours (07 CST to 09 CST) when the ozone in 1Hr-OA case is significantly better than the No-OA case due to much improved winds.

		No-OA		1Hr-OA	
	N	Corr	IOA	Corr	IOA
Hr|All	1150	0.79	0.86	0.81	0.88
0	48	0.04	0.30	0.40	0.46
1	43	0.20	0.24	0.36	0.30
2	48	0.14	0.25	0.35	0.35
3	48	0.19	0.30	0.32	0.35
4	48	0.27	0.36	0.31	0.35
5	47	0.24	0.36	0.28	0.37
6	47	0.33	0.38	0.35	0.37
7	**48**	**0.06**	**0.39**	**0.29**	**0.47**
8	**48**	**0.09**	**0.43**	**0.53**	**0.63**
9	**47**	**0.05**	**0.41**	**0.55**	**0.74**
10	47	−0.10	0.29	0.30	0.51
11	47	0.13	0.39	−0.07	0.36
12	49	0.09	0.38	0.25	0.40
13	49	−0.09	0.37	0.36	0.46

ACPD
15, 27357–27404, 2015

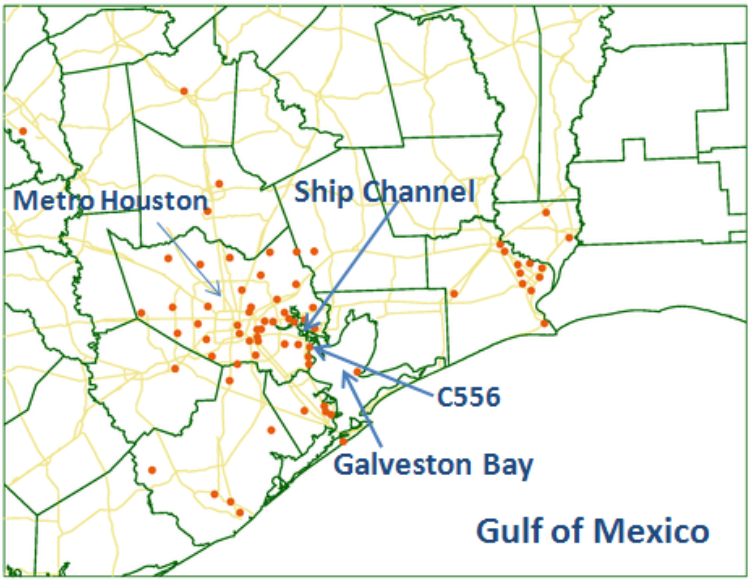

Figure 1. Locations of CAMS sites (dots) in CMAQ 4 km modeling domain during September 2013. Metro Houston, Houston Ship Channel, Galveston Bay and Gulf of Mexico are labeled.

ACPD
15, 27357–27404, 2015

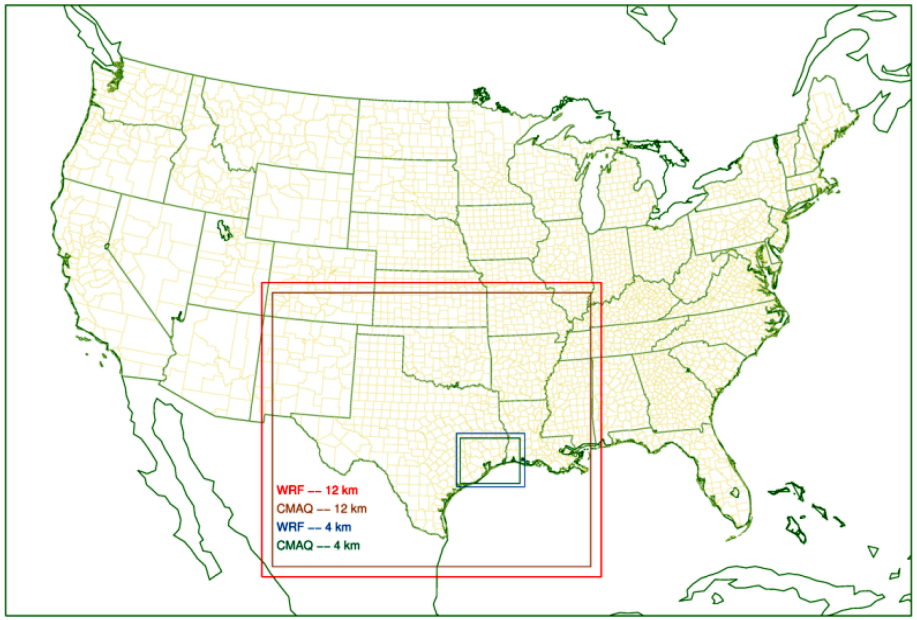

Figure 2. Horizontal domains of WRF and CMAQ simulation at 4km and 12 km grid resolution (the bigger domains are for 12km WRF and CMAQ and the smaller domains for 4 km WRF and CMAQ).

ACPD
15, 27357–27404, 2015

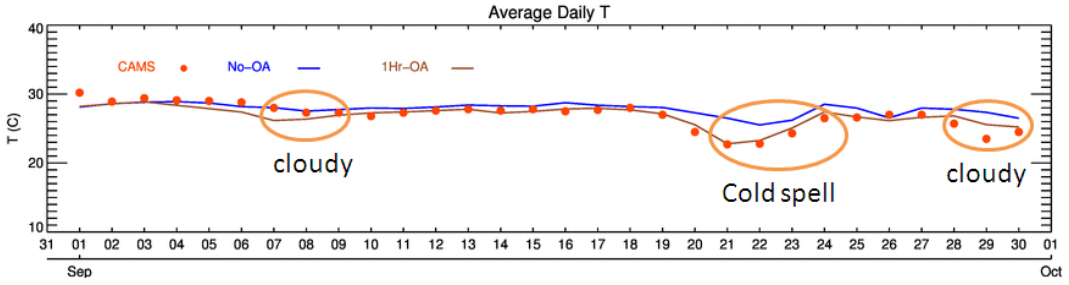

Figure 3. Regional daily temperature averaged over all available (typically around 1200) hourly CAMS observations for September of 2013.

ACPD
15, 27357–27404, 2015

The impact of observation nudging on simulated meteorology

X. Li et al.

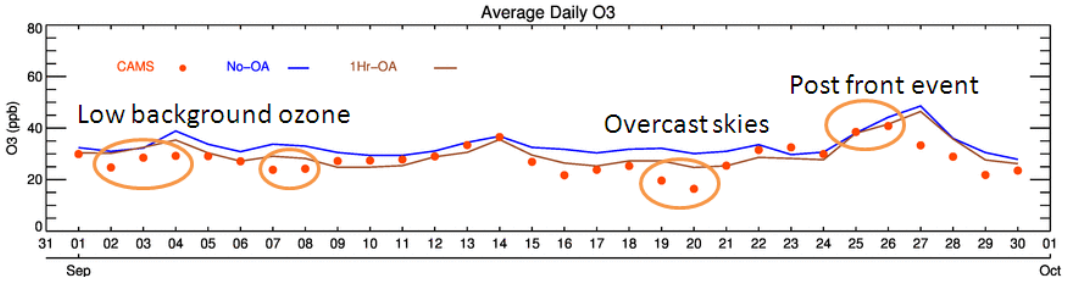

Figure 4. The daily regional averaged ozone for the two cases (No-OA and 1hr-OA) at the stations which include observation surface O_3 over the 4 km domain for September of 2013.

ACPD
15, 27357–27404, 2015

The impact of observation nudging on simulated meteorology

X. Li et al.

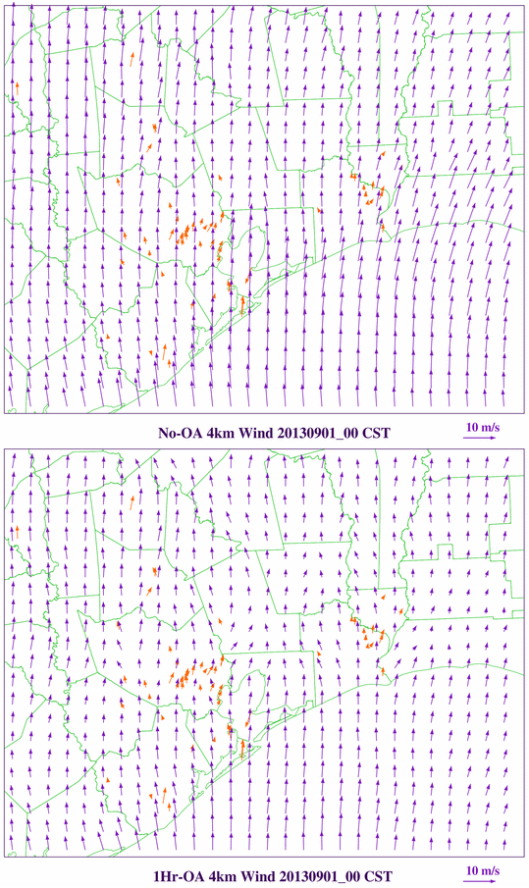

Figure 5. Model and observed winds at 09/01_00 CST: No-OA (top) and 1Hr-OA (bottom). Model winds are blue arrows and the observations are orange arrows. Stronger southerly winds, especially along coastal region, were reduced in the OA case.

ACPD
15, 27357–27404, 2015

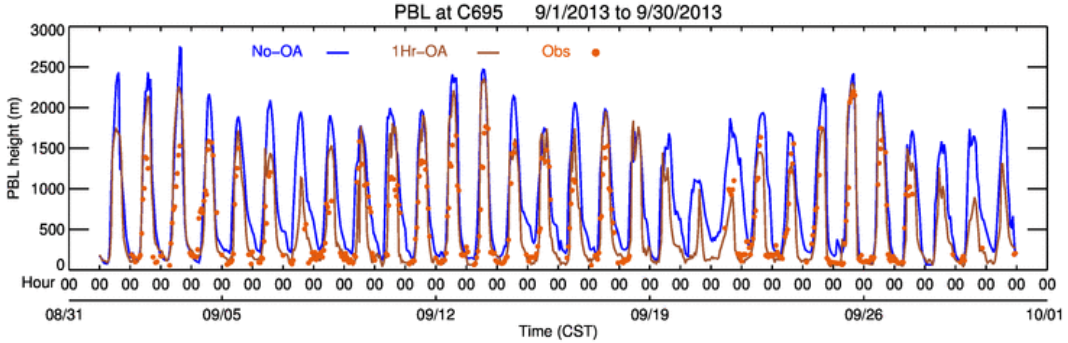

Figure 6. Planetary Boundary Layer (PBL) height time series at CAMS C695 for September 2013.

ACPD
15, 27357–27404, 2015

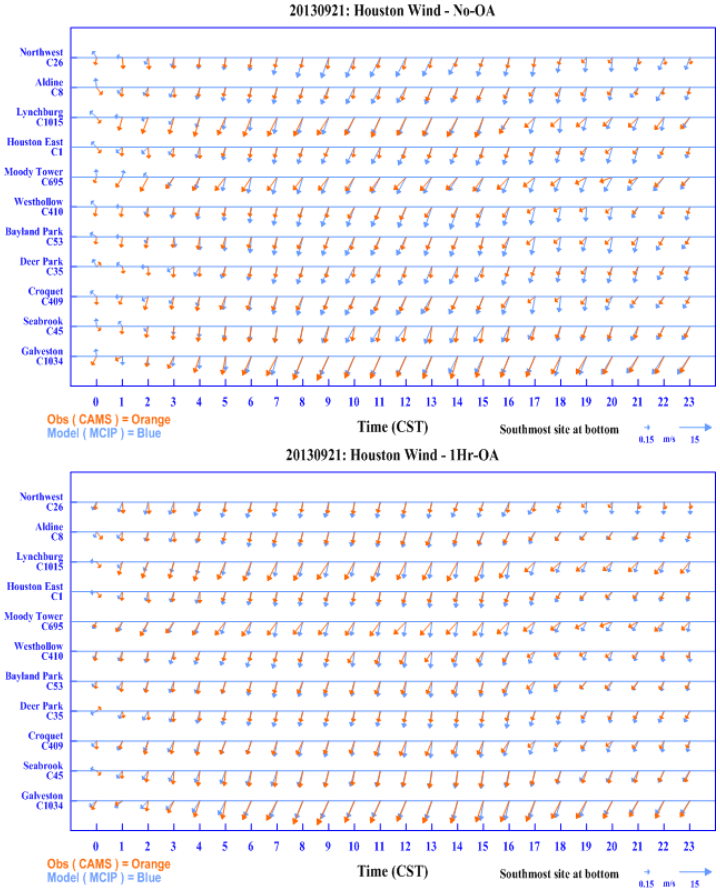

Figure 7. Hourly model (blue) and CAMS (orange) winds at 11 sites on 21 September: No-OA (top) and 1hr-OA (bottom). The 1hr-OA case is better in 00 CST to 02 CST and 17 CST to 20 CST.

ACPD
15, 27357–27404, 2015

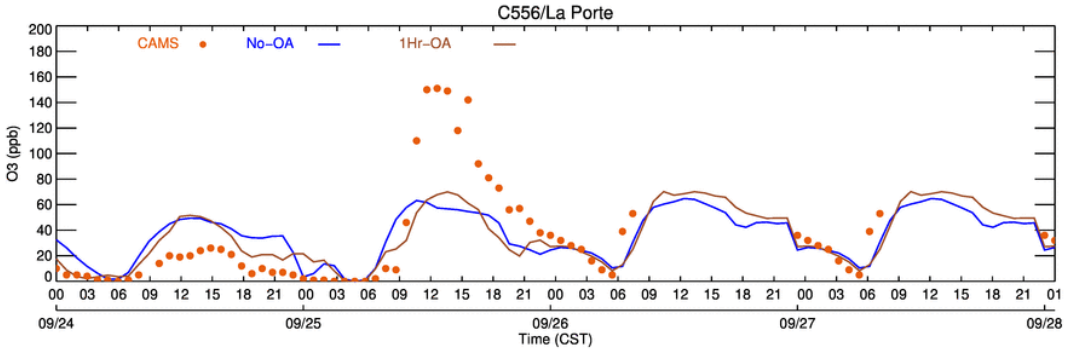

Figure 8. Ozone time series of La Porte (C556) between 09/24_00 to 09/28_00 CST of 2013.

ACPD
15, 27357–27404, 2015

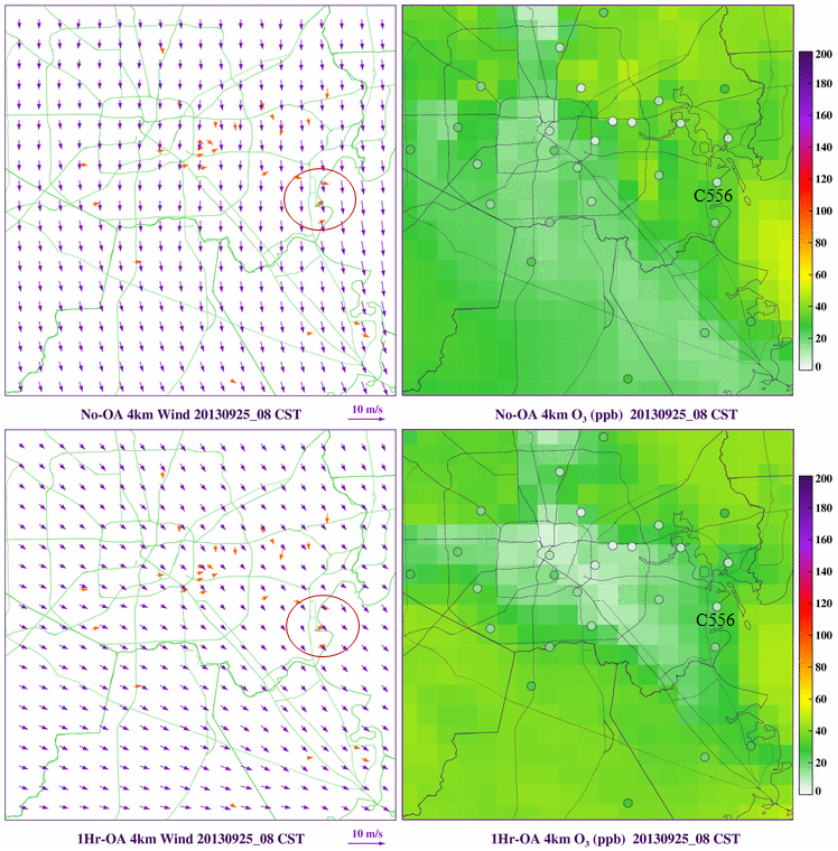

Figure 9. Zoom-in ozone concentrations (right) and wind plots (left) at 09/25_08 CST of 2013 for "No-OA" (top) and "1Hr-OA" (bottom). Ozone observation is in small circle; wind observation is indicated by an orange arrow. La Porte site C556 is labeled. The value range of right-side colour scale is 0 to 200 ppb. Higher value than 200 ppb has the same colour as 200 ppb.

ACPD
15, 27357–27404, 2015

The impact of observation nudging on simulated meteorology

X. Li et al.

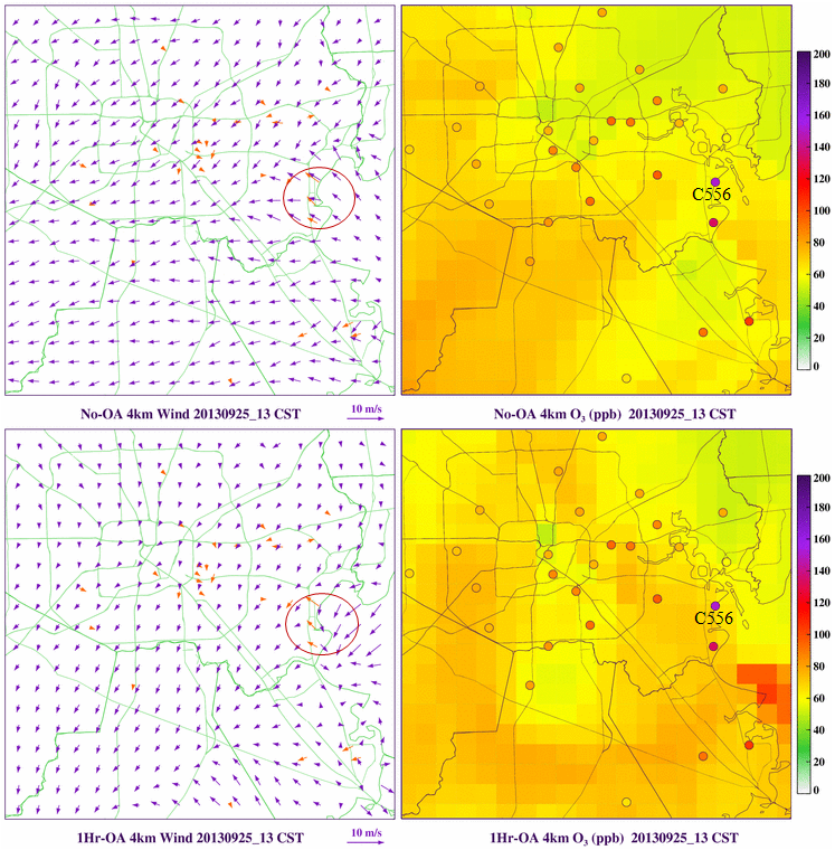

Figure 10. Zoom-in ozone concentrations (right) and wind plots (left) at 09/25_13 CST of 2013 for "No-OA" (top) and "1Hr-OA" (bottom). Ozone observation is in small circle; wind observation is indicated by an orange arrow. La Porte site C556 is labeled. Bay breeze is shown in the orange oval.

ACPD
15, 27357–27404, 2015

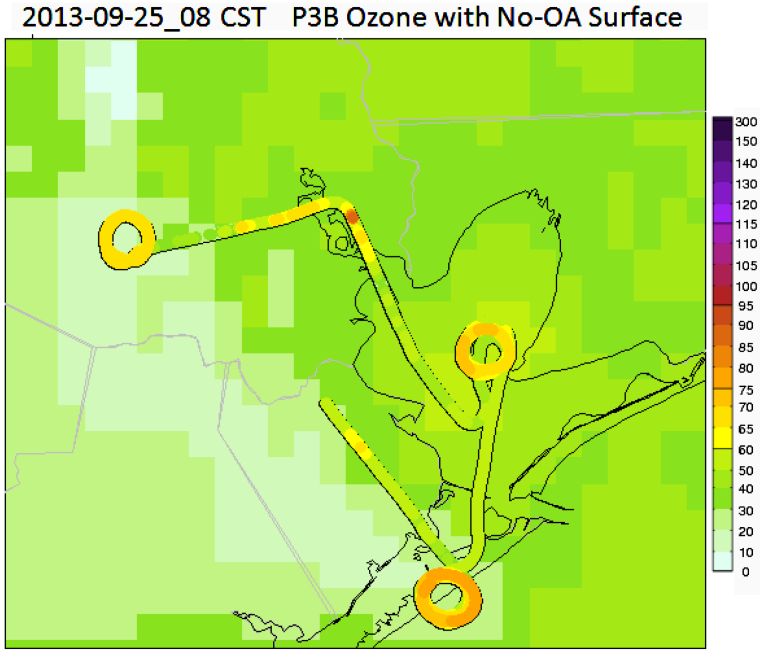

Figure 11. Ozone along aircraft tracks at 08 CST of September 25th, overlaid upon model No-OA surface ozone.

ACPD
15, 27357–27404, 2015

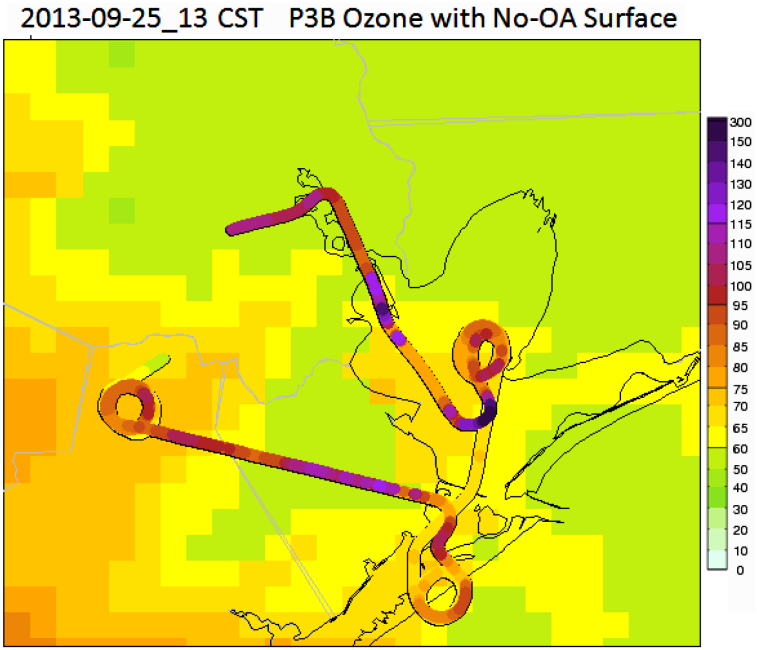

Figure 12. Ozone along aircraft tracks at 09/25_13 CST of 25 September, overlaid upon model "No-OA" surface ozone. Plumes can be seen as dark purple circles in Galveston Bay.

ACPD
15, 27357–27404, 2015

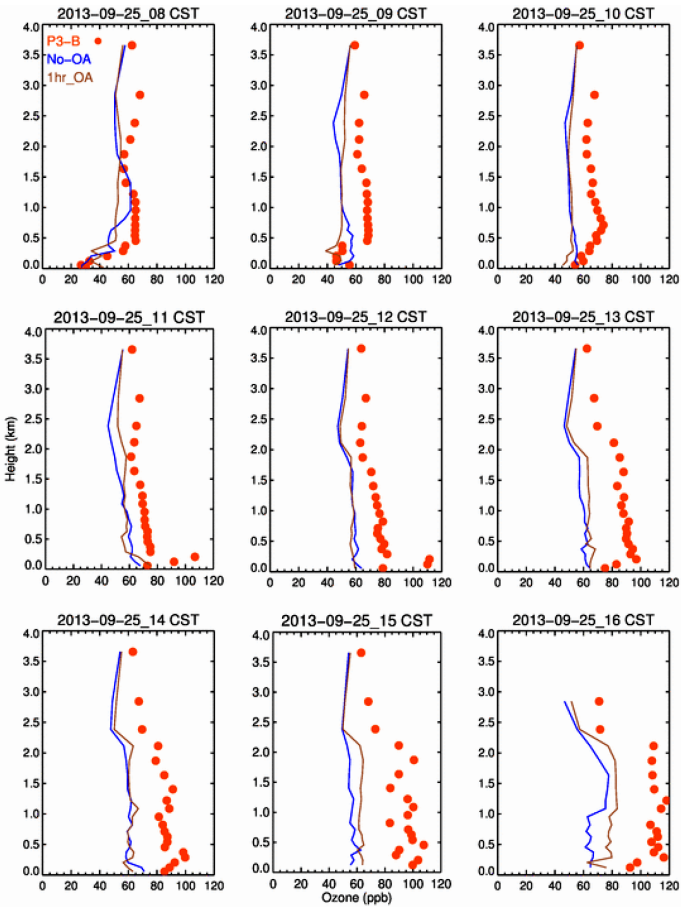

Figure 13. Vertical ozone profiles from 09/25_08 CST to 09/25_16 CST of 2013 for two cases of No-OA and 1Hr-OA compared with corresponding observations.

ACPD
15, 27357–27404, 2015

The impact of observation nudging on simulated meteorology

X. Li et al.

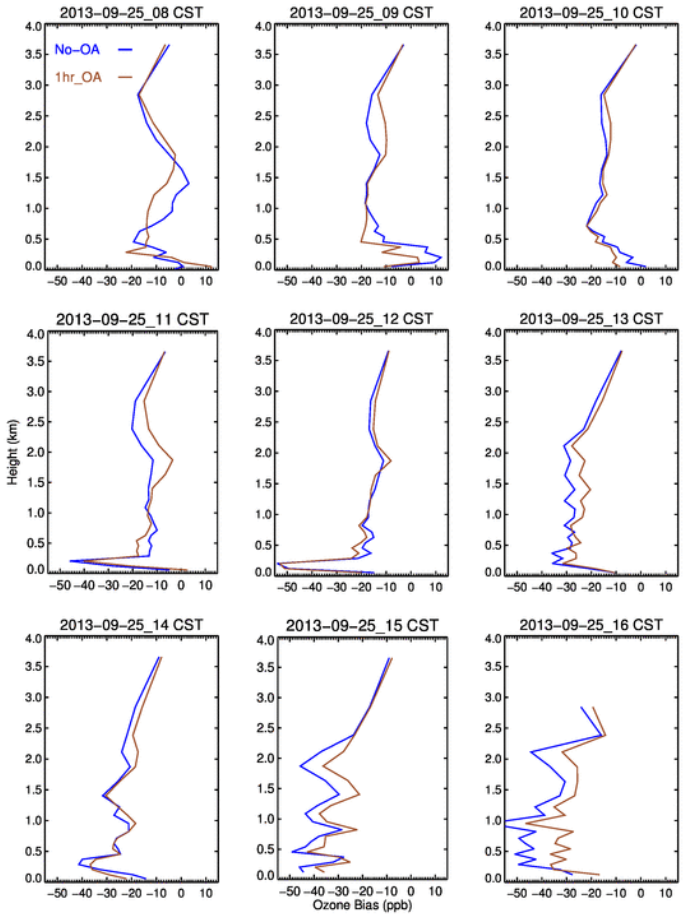

Figure 14. Model vertical ozone biases from 09/25_08 CST to 09/25_16 CST of 2013 for two cases of No-OA and 1Hr-OA.

ACPD
15, 27357–27404, 2015

The impact of observation nudging on simulated meteorology

X. Li et al.